Tensile and fatigue fracture mechanisms of a Zr-based bulk metallic glass

Z.F. Zhang,[a] J. Eckert,[b] and L. Schultz
IFW Dresden, Institute for Metallic Materials, P.O. Box 270016, D-01171, Dresden, Germany

The tensile and fatigue fracture behavior of $Zr_{59}Cu_{20}Al_{10}Ni_8Ti_3$ bulk metallic glass was investigated. It was found that under tensile load the metallic glass always displays brittle shear fracture and the shear fracture plane makes an angle of θ_T ($= 54°$) with respect to the stress axis, which obviously deviates from the maximum shear stress plane (45°). Under cyclic tension–tension loading, fatigue cracks first initiate along the localized shear bands on the specimen surface, then propagate along a plane basically perpendicular to the stress axis. Tensile fracture surface observations reveal that fracture first originates from some cores, then propagates in a radiate mode, leading to the formation of a veinlike structure and final failure. The fatigue fracture processes of the specimens undergo a propagation stage of fatigue cracks followed by catastrophic failure. Based on these results, a tensile fracture criterion for bulk metallic glasses is proposed by taking the effect of normal stress into account. It is suggested that both normal and shear stresses affect the fracture process of metallic glasses and cause the deviation of the fracture angle away from 45°.

I. INTRODUCTION

Bulk metallic glasses (BMGs) have a unique combination of properties that makes them potentially attractive structural materials;[1,2] however, the high strength of BMGs is often accompanied by remarkably little plastic deformation.[3–12] To improve the mechanical properties of BMGs, several efforts have been made by different approaches, such as precipitation of nanoscale particles by partial crystallization[13–15] and homogenous dispersion of insoluble particles or fibers as reinforcements.[16–18] Another recently developed technique is to precipitate dendritic crystals *in situ*, which results in ductile BMG composites containing microsized particles.[19,20] New BMG composites containing different reinforcements are being investigated and developed for potential industrial application.

On the other hand, for the fabrication of the BMGs with excellent performance, it is necessary to reveal their basic deformation and fracture mechanisms. As is known, in crystalline materials, slipping, shearing, kinking, and twinning are important plastic deformation modes,[21] and the yielding of most single crystals often follows the Schmid law. In general, single crystals will slide along the slip system with the largest Schmid factor; therefore the yield stress, the angle θ between slip bands and the stress axis can be calculated from the orientation of the single crystal. For metallic glasses, their plastic deformation mainly localized in narrow shear bands, followed by the rapid propagation of those shear bands and sudden fracture.[3–12] It is widely noted that under compressive loading, metallic glasses often fracture along the localized shear bands and the fracture angle θ_C between the compressive axis and the shear plane is smaller than 45° (about 42°).[10–12,22–26] Under tensile load, however, the tensile fracture angle θ_T between the tensile axis and the shear plane is in general larger than 45°. In most cases, θ_T is in the range of 51–60°, and the average value is about 56°.[5,22–28] This indicates that there is no definite shear plane as in crystalline materials for the formation of shear bands in metallic glasses. Also, the deformation and fracture of metallic glasses does not occur along the maximum shear stress plane no matter whether the glass is under tensile or compressive loading.

Among the mechanical properties of metallic glasses, the fatigue behavior has received less attention and is poorly understood.[29–37] Recently, fatigue behavior of several metallic glasses was preliminarily investigated, however, the basic fatigue damage mechanism was not considered in those experiments.[29–37] Accordingly, the difference in the fatigue cracking mechanisms between metallic polycrystals and amorphous materials is not yet

---

[a] On leave from Shenyang National Laboratory for Materials Sciences, Institute of Metal Research, Chinese Academy of Science, Shenyang, 110016, People's Republic of China.
e-mail: z.f.zhang@ifw-dresden.de

clear. For example, it is well known that fatigue cracks can nucleate along persistent slip bands (PSBs)[38,39] or deformation bands[40,41] in fatigued single crystals. For bicrystals and polycrystals, grain boundaries are the preferential sites for the nucleation of fatigue cracks due to the piling-up of dislocations at the grain boundaries.[42–44] It is known that metallic glasses possess a high yield and fracture strength (approximately 1.5–2.0 GPa). The applied stress during cyclic deformation is generally far below their fracture strength;[29,31,35–37] however, it is not clear whether shear bands form during cyclic deformation of metallic glasses at a low stress level. Another interesting question is where fatigue damage in metallic glasses nucleates because there are no grain boundaries in amorphous materials. Therefore, in the present work, we attempted to study the basic deformation and fracture mechanism of metallic glasses through tensile and fatigue tests of a $Zr_{59}Cu_{20}Al_{10}Ni_8Ti_3$ bulk metallic glass.

II. EXPERIMENTAL

Master ingots with composition $Zr_{59}Cu_{20}Al_{10}Ni_8Ti_3$ were prepared by arc-melting elemental Zr, Cu, Al, Ni, and Ti with a purity of 99.9% or better in a Ti-gettered argon atmosphere. Subsequently, the master ingots were remelted several times to achieve homogeneity, followed by casting into a copper mold with dimensions of 40 × 30 × 1.8 mm. The amorphous structure of the samples was verified by standard x-ray diffraction (XRD; Philips PW1050 diffractometer using Co K_α radiation). As shown in Fig. 1, the samples show only broad diffraction maxima, and no peaks of any crystalline phase can be seen, revealing the amorphous structure of the samples. Tensile and fatigue specimens with a total length of 40 mm were machined from the plates and polished to produce a mirror surface. The final gauge dimension for all the specimens is about 6 × 3 × 1.5 mm. Tensile deformation was conducted in a strain rate range of 3×10^{-5}
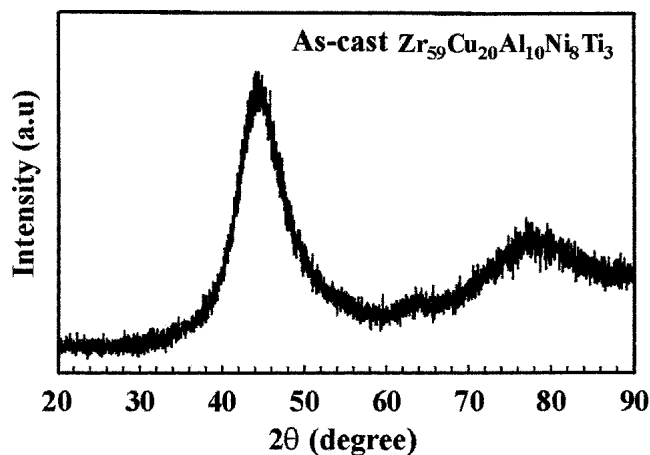
to 3×10^{-2} s^{-1} with an Instron 4466 testing machine at room temperature. Cyclic tension–tension tests were performed under stress control. The ratio of the maximum tensile stress σ_{max} to the tensile fracture stress σ_F was in the range of 0.5–0.8 at a constant stress ratio $R = \sigma_{min}/\sigma_{max} = 0.1$. A triangle wave with a frequency of 1 Hz was used for all the fatigue tests. After fracture, all the specimens were investigated with a JEOL JSM 6400 scanning electron microscope (SEM) and an optical microscope (OM) to reveal the fracture surface morphology.

III. RESULTS

A. Tensile stress–strain curves

Figure 2 shows the stress–strain curves of the glassy specimens obtained at different strain rates. All the specimens display only elastic deformation behavior and subsequent catastrophic fracture without yielding. For better visibility, the curves are shifted along the strain axis. The fracture stress σ_F of the four specimens nearly has the same value of 1.58 ± 0.02 GPa, independent of the applied strain rate. The Young's modulus is 91.1 ± 1.8 GPa, and the total strain before failure is about 1.8%. These results agree well with the literature data reported for Zr–Cu–Al–Ni–Ti glasses.[45] The independence of the fracture stress on the strain rate was also observed for other metallic glasses.[28,46] Figure 3 shows the dependence of fracture stress σ_F on the applied strain rate for the present alloy as well as $Pd_{40}Ni_{40}P_{20}$ and $Zr_{65}Al_{10}Ni_{10}Cu_{15}$ metallic glasses.[28,46] For the three metallic glasses, the tensile fracture stress is always constant for different strain rates. This indicates that the fracture strength of these metallic glasses is insensitive to the applied strain rate.

B. Fatigue life curves

Figure 4 gives the fatigue life curves of the present alloy and $Zr_{55}Cu_{30}Al_{10}Ni_5$ metallic glass[31] subjected to cyclic tension–tension loading. It can be seen that the
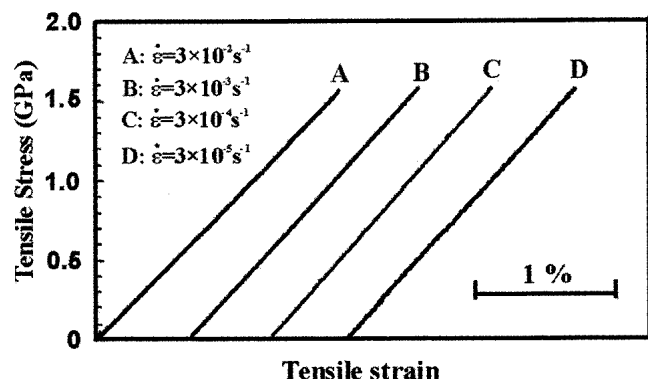

FIG. 1. XRD pattern for $Zr_{59}Cu_{20}Al_{10}Ni_8Ti_3$ metallic glass.

FIG. 2. Tensile stress-strain curves for $Zr_{59}Cu_{20}Al_{10}Ni_8Ti_3$ metallic glassy specimens at different strain rates ranging from 3×10^{-5} to 3×10^{-2} s^{-1}.

average fatigue life N_f of the present alloy is slightly lower than that of $Zr_{55}Cu_{30}Al_{10}Ni_5$ metallic glass in the range of $\sigma_{min}/\sigma_{max} = 0.5$ to 0.8. One reason for this can be attributed to the difference in the stress ratio R since $Zr_{55}Cu_{30}Al_{10}Ni_5$ metallic glass was applied cyclic tension–tension loading under $R = 0.5$.[31] Thus, at the present stress ratio $R = 0.1$, the cyclic stress amplitude $\sigma_a = (\sigma_{max} - \sigma_{min})/2$ is obviously higher than that under $R = 0.5$ for the same maximum stress σ_{max}. Another feature of Fig. 4 is that, in the range of $\sigma_{max}/\sigma_F = 0.5$ to 0.8, the value of log (N_f) nearly decreases linearly with increasing σ_{max}/σ_F. The corresponding fatigue life N_f for the two metallic glasses is in the range of 10^3 to 10^4, which is a typical low-cycle-fatigue (LCF) life range for crystalline materials. As is well known for crystalline materials, the LCF damage mechanism will mainly be controlled by the plastic deformation.[47] However, for metallic glasses, the LCF damage mechanism is still unclear[29–37] and will be discussed in the following sections.
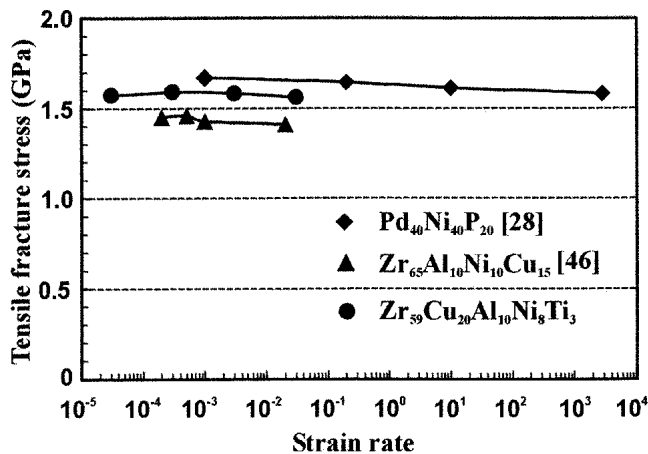

FIG. 3. Dependence of fracture strength on the strain rate for the present alloy, $Pd_{40}Ni_{40}P_{20}$[28] and $Zr_{65}Ali_{10}Ni_{10}Cu_{15}$[46] metallic glasses.
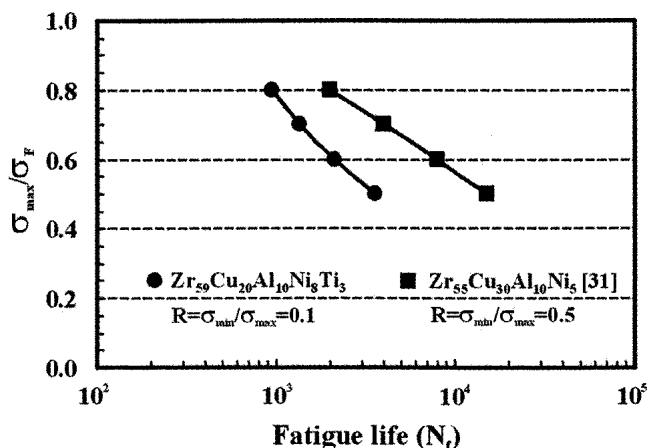

FIG. 4. Fatigue life curves for $Zr_{59}Cu_{20}Al_{10}Ni_8Ti_3$ and $Zr_{55}Cu_{30}Al_{10}Ni_5$[31] metallic glasses.

C. Tensile fracture surface observations

OM and SEM observations show that all the tensile specimens fractured in a shear mode, as shown in Fig. 5(a). The formation and propagation of one major shear band dominates the fracture process. The fracture surface is very smooth and a veinlike morphology can be easily seen [Fig. 5(b)], similar to what was observed for other metallic glasses.[24–27] The shear fracture surface makes an angle θ_T with respect to the stress axis on one surface; however, it is perpendicular to the stress axis on the adjacent surface. Therefore, the tensile fracture angle θ_T between the tensile axis and the fracture plane can be readily measured on the surface of the specimen, as marked in Fig. 5(a). The tensile fracture angle θ_T of the present glass is equal to 54°, rather than 45°. This result is consistent with previous observations for the other metallic glasses under tensile deformation.[5,22–28] For comparison, all the available results about θ_T are listed in Table I. It can be seen that, in general, θ_T is in the range of 53–65° for different metallic glasses, which deviates from the maximum shear stress plane. Therefore, it can be concluded that the tensile deformation behavior of metallic glasses should not follow the von Mises criterion,[11] and a new deformation mechanism must play an important role in the fracture process of metallic glasses.

Further observations show that the morphology on the tensile fracture surface is quite peculiar in comparison with that on the compressive fracture surfaces. Besides the veinlike structure on the tensile fracture surface, there are many cores with different diameters, as shown in Figs. 5(c)–5(f). However, these cores were never previously mentioned in detail for metallic glasses subjected to tensile deformation. There are some similar features appearing on tensile fracture surfaces, such as given in Ref. 5 (Figs. 8 and 13), Ref. 28 (Fig. 5), and Ref. 48 (Fig. 8). All the micrographs demonstrate that the cores coexist with the veins and all the veins radiate away from these cores. In the region of the cores, the fracture seems to take place in a normal fracture mode, rather than a pure shear mode. The present fracture feature is distinctly different from that on the compressive fracture surface of metallic glasses since the vein always arranges nearly along the same direction, showing a pure shear fracture feature. This indicates the loading modes strongly affect the fracture mechanism of metallic glasses. For better understanding the formation mechanism of these cores, the tensile fracture surface will be further investigated by transmission electron microscopy as observed by Gao et al.,[49] and the corresponding results will be reported elsewhere.

D. Fatigue fracture surface observations

Figure 6(a) shows the fatigue fracture surface of the metallic glass specimen at $\sigma_{max}/\sigma_F = 0.6$. The whole fatigue fracture surface is somewhat rough in comparison
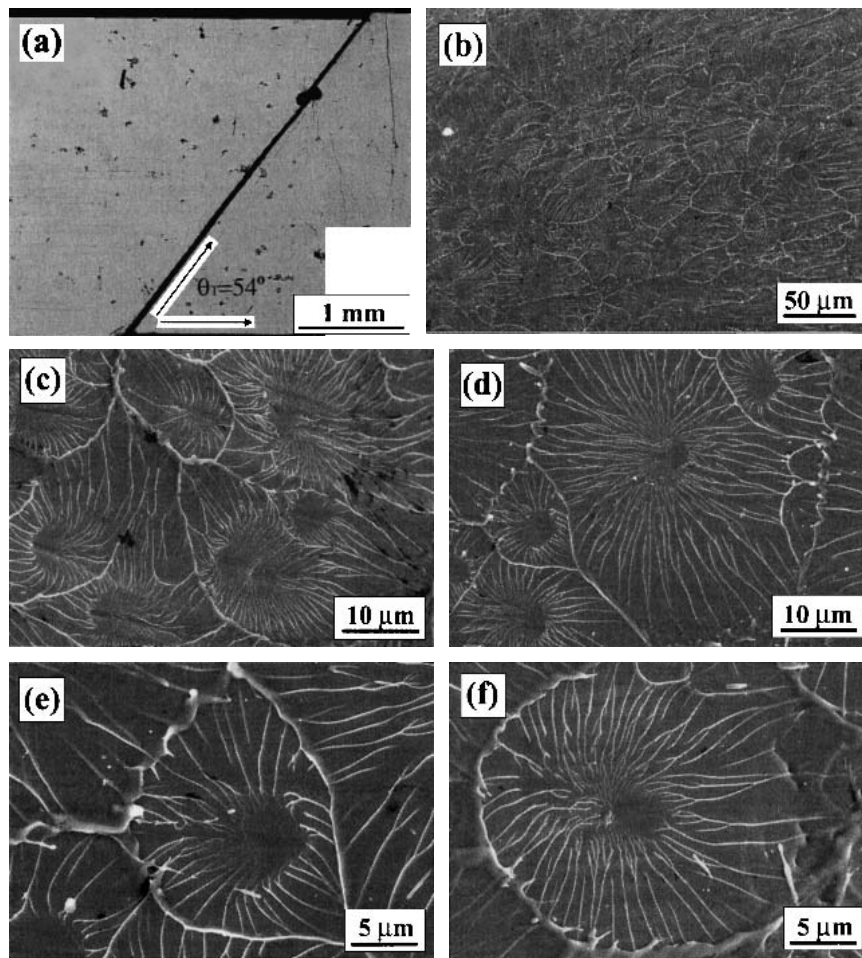
FIG. 5. OM and SEM micrographs revealing (a) the tensile fracture of $Zr_{59}Cu_{20}Al_{10}Ni_8Ti_3$ metallic glass and (b–f) the fracture surface morphology at different magnifications.

TABLE I. Comparison of the tensile fracture angle θ_T for different metallic glasses.

Investigators	Metallic glasses	Fracture angle (θ_T)
Pampillo[5]	$Pd_{80}Si_{20}$	$\theta_T = 54.7°$
Takayama[22]	$Pd_{77.5}Cu_6Si_{16.5}$	$\theta_T = 51°$
Lowhaphandu *et al.*[23]	$Zr_{62}Ti_{10}Ni_{10}Cu_{14.5}Be_{3.5}$	$\theta_T = 57 \pm 3.7°$
Wright *et al.*[24]	$Zr_{40}Ti_{14}Ni_{10}Cu_{12}Be_{24}$	$\theta_T = 56°$
He *et al.*[25]	$Zr_{52.5}Ni_{14.6}Al_{10}Cu_{17.9}Ti_5$	$\theta_T = 55$ to $65°$
Inoue *et al.*[26]	$Cu_{60}Zr_{30}Ti_{10}$	$\theta_T = 54°$
Liu *et al.*[27]	$Zr_{52.5}Ni_{14.6}Al_{10}Cu_{17.9}Ti_5$	$\theta_T = 53$ to $60°$
Mukai *et al.*[28]	$Pd_{40}Ni_{40}P_{20}$	$\theta_T = 56°$
Present results	$Zr_{59}Cu_{20}Al_{10}Ni_8Ti_3$	$\theta_T = 54°$

with the tensile fracture surface. The fracture surface is basically perpendicular to, rather than inclined to, the loading direction. At one corner of the specimen (marked by A), a fatigue crack originates and propagates towards the opposite corner. The propagation path of the fatigue crack is roughly perpendicular to the stress axis and the propagation region is relatively flat, as marked in region B. Besides the propagation region, the other part of the

fracture surface corresponds to the final fast fracture region of the specimen, which shows a shear plane tilted to the stress axis, as marked by C. A similar fatigue fracture behavior was also observed in other fatigued metallic glasses.[29,31,34,35] Figure 6(b) demonstrates several shear bands with different angles to the stress axis on the specimen surface, indicating that shear bands have formed during cyclic deformation even though the applied maximum tensile stress σ_{max} is obviously lower than the tensile fracture stress σ_F. This result proves that the stress for formation of shear bands in metallic glass is lower than the fracture stress during cyclic loading. A similar feature was also observed for $Zr_{57}Cu_{20}Al_{10}Ni_8Ti_5$ metallic glass during bending.[49] However, it is worth noting that shear bands did not transfer through the whole section of the specimen but terminated at a certain distance from the surface. Besides the primary shear bands, some secondary shear bands originated from the primary shear bands. Both primary and secondary shear bands are not straight. This deformation feature is quite different from the slip bands in crystalline materials, which have a strict
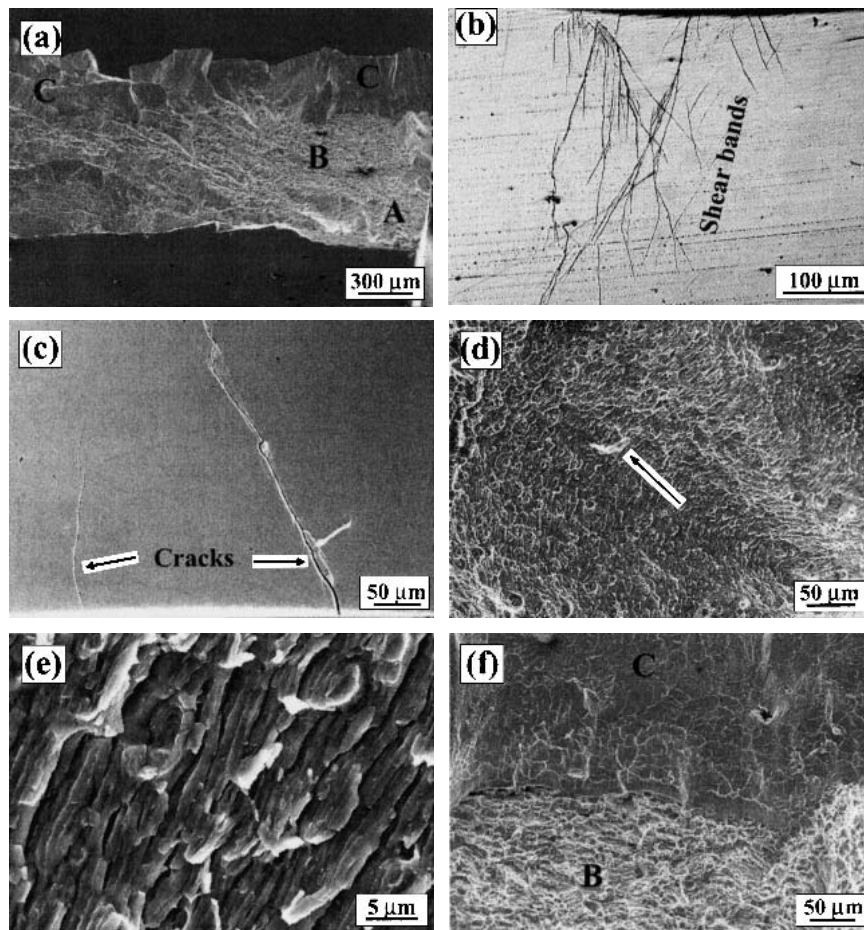
J. Mater. Res., Vol. 18, No. 2, Feb 2003

459

FIG. 6. (a) Overall fatigue fractography of the glassy specimen at $\sigma_{max}/\sigma_F = 0.6$. (b) Surface shear bands and (c) fatigue crack developed from the shear bands. (d) Fatigue-crack propagation region at low magnification and (e) at high magnification. (f) Boundary between propagation region and final fast fracture region.

crystallographic plane. The shear deformation feature in metallic glasses should be attributed to its amorphous structure. With further cyclic deformation, some of the shear bands develop into a fatigue crack, as shown in Fig. 6(c). Initially, the fatigue crack propagates along the shear bands, then proceeds along a plane basically perpendicular to the loading direction, resulting in a fatigue fractography, as shown in Fig. 6(a). When the fatigue-crack propagation region is observed, one can see that the fracture surface morphology is similar to the fatigue striations in fatigued crystalline materials,[47] as shown in Figs. 6(d) and 6(e). However, this fracture feature is quite different from that observed on the tensile fracture surface in Figs. 5(b)–5(f). On the fatigue fractography, there is no indication for a vein-like structure, induced by the rapid fracture process.[27] This reveals a significant difference between tensile and fatigue fracture mechanisms. At the end of the propagation region, there is a distinct boundary between the two regions, as shown in Fig. 6(f). The final fracture surface shows a clear veinlike structure, which is identical with the tensile fracture surface.

IV. DISCUSSION

A. Tensile fracture mechanism of metallic glasses

From the above morphology, one can deduce that the fracture of metallic glass first originates from those cores induced by normal tension stress on a plane, then catastrophically propagates away from the cores in a shear mode driven by the shear stress, resulting in the formation of the radial veins on the fracture surface. Hence, we propose a new possible fracture process for the metallic glassy specimen, as illustrated in Figs. 7(a)–7(c). Since the cores always appear on the whole fracture surface, Fig. 7(a) demonstrates the initial stage of nucleation of the cores induced by the normal tension stress σ_θ. Once these cores form, they will propagate rapidly driven by the shear stress τ_θ and connect with each other, as illustrated in Fig. 7(b). Finally, the rapid propagation of the cores results in catastrophic fracture. Thus, some cores and the veinlike structure appear on the fracture surface, as illustrated in Fig. 7(c), which is consistent with the
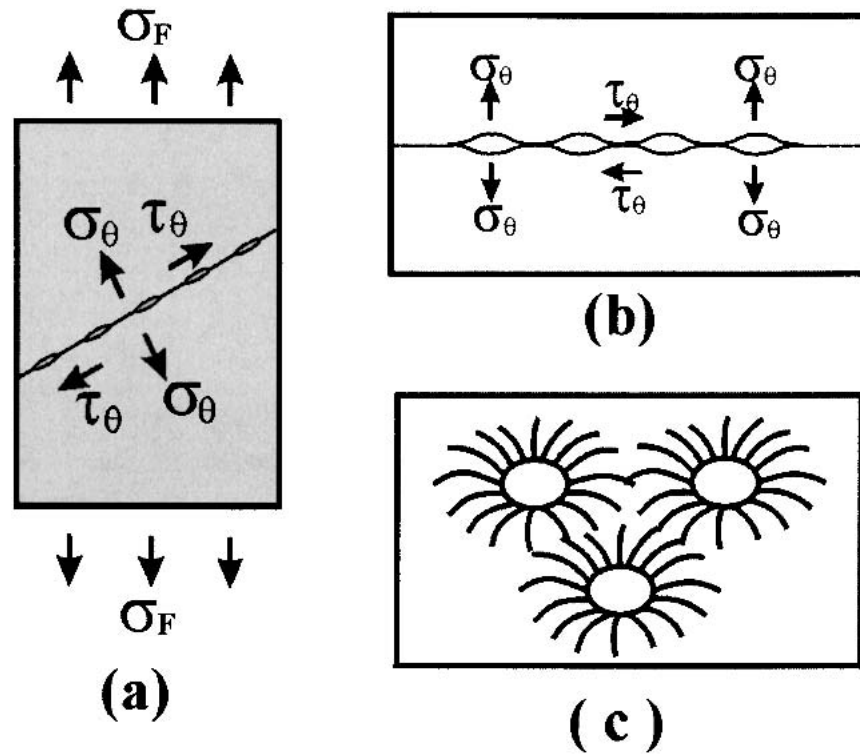
FIG. 7. Illustration of the fracture processes of a specimen under tensile deformation: (a) nucleation of cores, (b) propagation of cores, and (c) cores and veinlike structure.

observations in Figs. 5(b)–5(f). Therefore, it can be concluded that the fracture processes of a metallic glass subjected to tensile deformation should be controlled by both normal tension stress σ_θ and the shear stress τ_θ. After the nucleation of these cores, the fracture process will be mainly driven by the shear stress to produce the veinlike structure.

Since metallic glass is a homogenous material, we may assume that there are two critical fracture stresses, i.e., σ_0 and τ_0, as illustrated in Figs. 8(a) and 8(b). σ_0 can be

defined as the critical normal fracture stress on any plane under the condition without shear stress; τ_0 can be regarded as the critical shear fracture stress on any plane under the condition without normal stress. For a given metallic glass, σ_0 and τ_0 should be constants on any plane because of the isotropic amorphous structure. Therefore, the ratio of τ_0 to σ_0 should also be a constant, i.e., $\mu = \tau_0/\sigma_0$. Since metallic glasses have high fracture strengths σ_F (approximately 1.5–2.0 GPa), the applied normal stress σ_θ on the fracture plane is also very high
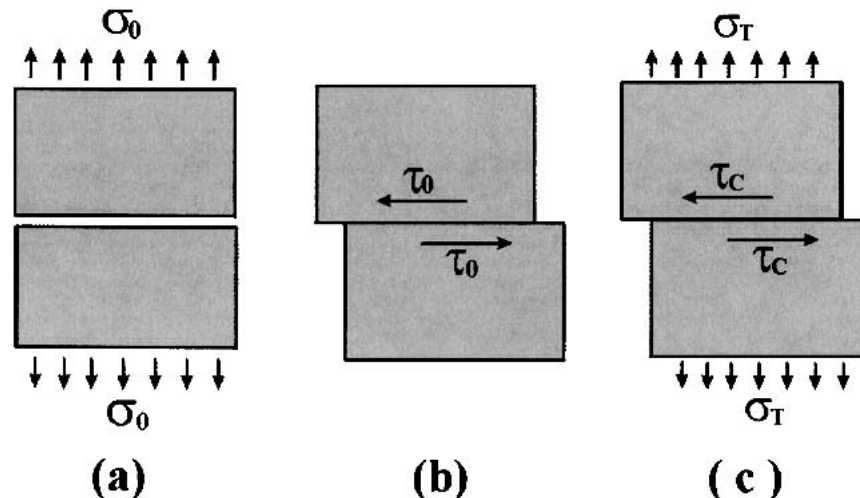

FIG. 8. Illustration of critical stresses of metallic glass: (a) critical normal fracture stress σ_0; (b) critical shear fracture stress τ_0, and (c) critical shear stress τ under the condition with normal tension stress σ_T.

(approximately 1.0 GPa) and therefore must play an important role in the fracture mechanism. The observations provide supportive evidence. The first is the deviation of the tensile fracture angle θ_T from the maximum shear stress plane (45°) in different metallic glasses,[5, 22–28] as listed in Table I. The second is the formation of the cores on the fracture surface, as observed in Figs. 5(b)–5(f). Therefore, if a metallic glass is subjected to a normal tension stress σ_T on a plane, as illustrated in Fig. 8(c), the applied stress necessary for normal fracture on this plane should be reduced to $(\sigma_0 - \sigma_T)$. Therefore, when metallic glass is subjected to a normal tension stress σ_T, the applied shear stress τ_c necessary for shear fracture along the plane should follow the equation below:

$$\frac{\tau_c}{\sigma_0 - \sigma_T} = \mu = \frac{\tau_0}{\sigma_0} \quad . \tag{1}$$

The present criterion also considers the effect of normal stress σ_T, as the Mohr–Coulomb criterion proposed by Donvonan.[9,11] For a glassy specimen under tensile loading, as illustrated in Fig. 9 and according to Eq. (1), the critical condition for shear fracture on the plane can be expressed as

$$\tau_\theta \geq (\sigma_0 - \sigma_\theta) \times \mu \quad . \tag{2}$$

Here, σ_θ and τ_θ are the normal and shear stresses on the shear plane and can be expressed as

$$\sigma_\theta = \sigma_F \times \sin^2(\theta) \quad , \tag{3}$$
$$\tau_\theta = \sigma_F \times \sin(\theta)\cos(\theta) \quad .$$

The variation of σ_θ and τ_θ with the shear angle θ can be illustrated as in Fig. 10. Substituting σ_θ and τ_θ into Eq. (2), one gets:

$$\sigma_F \geq \frac{\mu \times \sigma_0}{\sin(\theta) \times [\cos(\theta) + \mu \times \sin(\theta)]} \quad . \tag{4}$$

Since σ_0 and μ are constants, as illustrated in Fig. 10, the critical fracture stress σ_F should be a function of the shear angle θ and approaches a minimum value according to

$$\frac{\partial(1/\sigma_F)}{\partial\theta} = \frac{1}{2\mu\sigma_0}[\cos(2\theta) + \mu\sin(2\theta)] = 0 \quad . \tag{5}$$

Under this condition, metallic glasses should preferentially fracture along a favorable shear plane at the minimum applied stress σ_F. Therefore, the minimum applied fracture stress σ_F must correspond to the measured tensile fracture angle θ_T, as marked in Fig. 10. For the present metallic glass, $\sigma_F = 1.58$ GPa, $\theta_T = 54°$,

the three constants σ_0, τ_0, and μ can be calculated from Eqs. (4) and (5). The results are $\sigma_0 = 3.35$ GPa, $\tau_0 = 1.09$ GPa, and $\mu = 0.324$.

From Eq. (5), it is noted that θ_T strongly depends on the ratio $\mu = \tau_0/\sigma_0$, and increases with increasing μ. According to the above definition, σ_0 reflects the ability of a metallic glass to resist normal tensile fracture, and τ_0
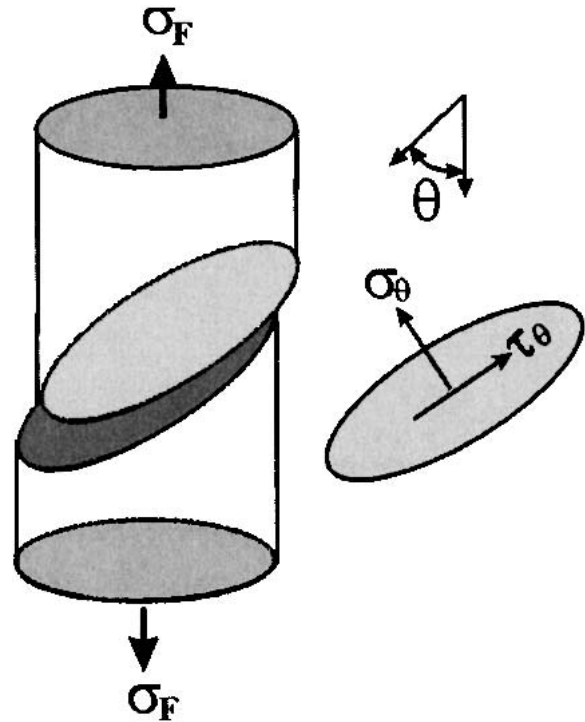

FIG. 9. Illustration of the tensile fracture specimen of the metallic glass.
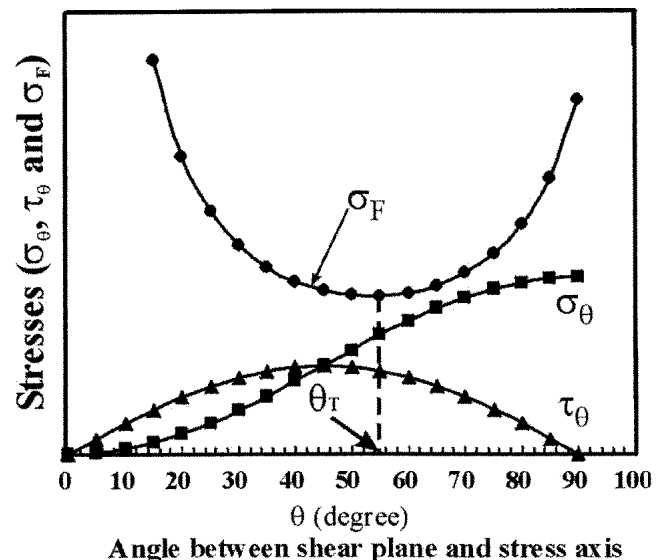

Angle between shear plane and stress axis

FIG. 10. Illustration of the variation of the normal and shear stresses on the fracture plane of a specimen under tensile deformation.

represents the critical resistance to shear fracture. As illustrated in Fig. 11 and Eq. (2), it is clear that with increasing applied tensile stress σ, the resolved shear stress τ_θ increases linearly. However, the critical shear fracture stress $\tau_c = \mu(\sigma_0 - \sigma_\theta)$ decreases gradually. When τ_θ reaches the critical value of τ_c, the critical fracture condition will be satisfied. This will correspond to the tensile fracture stress σ_F, as marked in Fig. 11. Meanwhile, the normal stress σ_θ increases rapidly with increasing shear angle θ, as illustrated in Fig. 10, whereas, the shear stress τ_θ decreases slowly at $\theta \geqslant 45°$. Through
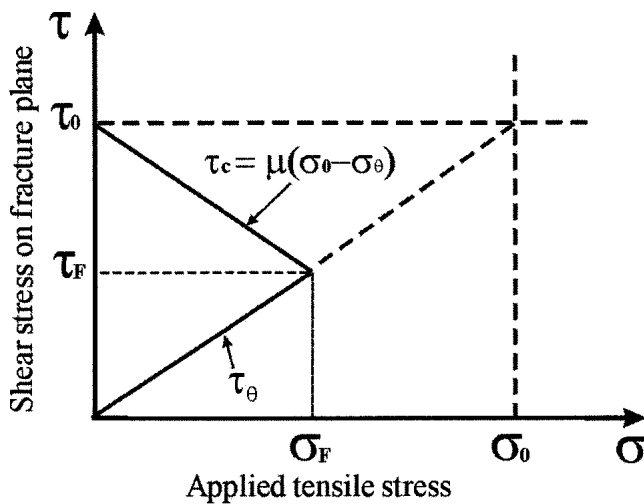

FIG. 11. Variation of the fracture stress σ_F, normal stress σ_θ and shear stresses τ_θ on the fracture angle under tensile deformation.

a combined effect of the normal and shear stresses, the fracture of metallic glasses often occurs along a favorable shear angle $\theta_t \geqslant 45°$ so as to approach the minimum critical value.

B. Fatigue fracture mechanism of metallic glasses

From the present observations of a fatigued $Zr_{59}Cu_{20}Al_{10}Ni_8Ti_3$ metallic glass, it can be concluded that its fatigue damage processes should include the following steps. First, shear bands form in the beginning of the fatigue damage process. The presence of a shear band in the glass reduces its strength by providing a site for further plastic flow. Under tensile deformation condition, metallic glasses usually develop a single shear band and fail by shear rupture through this band without measurable macroscopic plastic strain.[10] Under cyclic tension–tension loading, the applied maximum stress σ_{max} is obviously lower than the fracture strength σ_F of metallic glasses, for example, $\sigma_{max} = (0.5 - 0.8)\sigma_F$ in the present tests. At this low stress level, however, shear bands were also observed at local sites, as seen in Fig. 6(b). This result indicates that the formation of shear bands can occur at a stress level far below the fracture strength. Similarly, in a $Zr_{57}Cu_{20}Al_{10}Ni_8Ti_5$ metallic glass subjected to a three-point bend test, shear bands can form at a stress of about 80% (107N/136N) of the maximum stress.[50] In the present fatigue test, it is noted that the shear bands did not propagate through the whole section of the specimen but only distribute some local sites. This
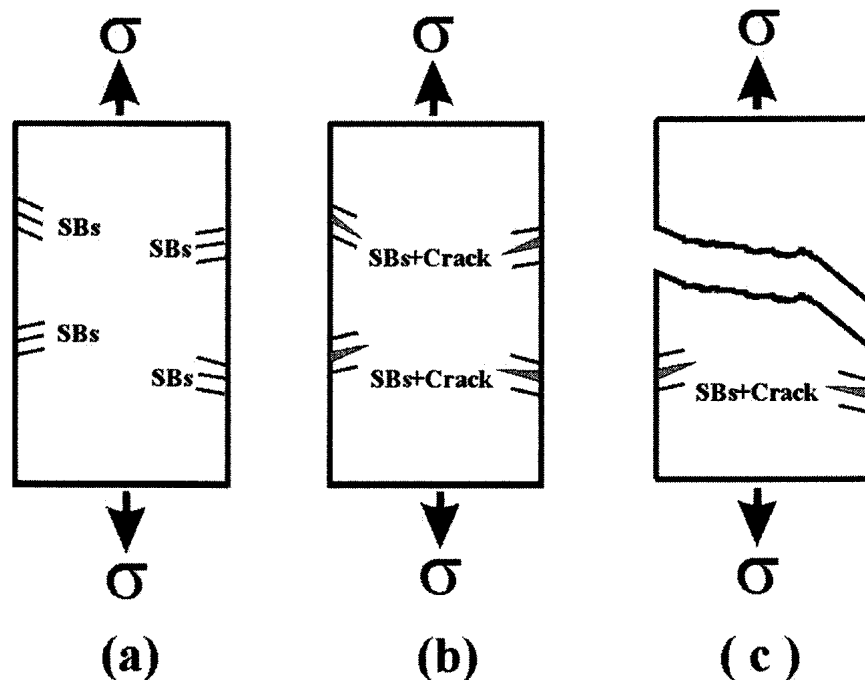

FIG. 12. Illustration of the fatigue fracture processes of the metallic glass specimen: (a) formation of shear bands at local site on the surface, (b) nucleation of fatigue crack along the localized shear bands, (c) propagation of fatigue crack and fatigue fracture of the specimen.

means that a stress concentration might exist, which results in the favorable nucleation of shear bands on the specimen surface, as illustrated in Fig. 12(a).

With further cyclic deformation, the fatigue crack can originate from the local shear bands, as shown in Fig. 6(c). This is similar to the PSB cracking mechanism in single crystals.[38–40] As is well known, the PSB cracking mechanism can be explained by the surface roughness induced by the irreversibility of PSBs.[38,39] However, as shown in Fig. 6(c), there is no such surface roughness near the shear bands on the specimen surface of the glass (as indicated by arrows). Therefore, the nucleation of a fatigue crack along the shear bands must be explained by another mechanism. Spaepen[6] proposed that within a narrow shear band there exists an excess free volume due to shear-induced disordering and diffusion controlled reordering. Therefore, the free volume usually refers to the fraction of matter having a lower atomic coordination than that in a reference material having dense random packing. Accordingly, the free volume region is mechanically weak relative to the surrounding volume.[7] Since a shear band is a relatively weak region in metallic glass, it can be regarded as the potential site for the nucleation of a fatigue crack. Under cyclic tension–tension loading, the gradual weakening, dilation, tearing, and the final opening of the shear band will result in the formation of a fatigue crack, as observed in Fig. 6(c) and illustrated in Fig. 12(b). Therefore, the nucleation of fatigue crack can be attributed to the weak nature within a shear band, which is independent of the surface roughness.

During cyclic deformation of metallic glass, there might be simultaneously several fatigue cracks along the shear bands. However, the cyclic stress might be only favorable for the propagation of a fatigue crack along one or two shear bands. In the end, the fatigue crack always propagates along the plane basically perpendicular to the loading direction, as demonstrated as in Fig. 12(c). Along the propagation path of the fatigue crack, however, there is no veinlike structure as observed in Figs. 6(d) and 6(e). This demonstrates that the melting phenomenon of metallic glass did not occur in the tip of the fatigue crack during the stable propagation stage. In turn, it means that the released elastic energy due to crack propagation is too low to melt the metallic glass locally. This result is consistent with observations reported in Refs. 30–33. Flores and Dauskardt have measured and predicted the temperature increase in the tip of a crack.[32] They found that in a $Zr_{41.25}Ti_{13.75}Ni_{10}Cu_{12.5}Be_{22.5}$ metallic glass the temperature increases only about 56.5 K, which provides indirect evidence for the fatigue fractography without the veinlike structure. However, in the final fast fracture region, the veinlike structure appears again and the fracture follows a shear mode, indicating that the fracture mechanism of the final region is identical with the tensile fracture.

V. CONCLUSIONS

Under tensile loading, $Zr_{59}Cu_{20}Al_{10}Ni_8Ti_3$ metallic glass displays a brittle shear fracture mode with a high fracture stress of 1.58 GPa, which is independent of the applied strain rate (3×10^{-5} to 3×10^{-2} s^{-1}). Its fracture does not obey the von Mises criterion since the fracture angle θ_T ($= 54°$) obviously deviates from the maximum shear stress plane ($45°$). On the fracture surface, there are many cores coexisting with a veinlike structure. Accordingly, the fracture first originates from the cores induced by the normal tension stress, then rapidly fracture in a pure shear mode. Based on these results, a new tensile fracture criterion for metallic glasses is developed by taking both the normal and shear stresses into account. Two critical fracture stresses, i.e., σ_0 and τ_0, were proposed, and the tensile fracture angle θ_T strongly depends on the ratio $\mu = \tau_0/\sigma_0$. It is suggested that the deviation of the tensile fracture angle θ_T away from $45°$ can be attributed to a combined effect of the normal and shear stresses on the fracture plane.

Under cyclic tension–tension loading, shear bands form at a stress level far below the tensile fracture stress. The fatigue crack first initiates along the shear bands on the surface, then propagates along a plane basically perpendicular to the loading direction. The fracture surface can be divided into two regions, i.e., propagation region and final fast fracture region. The fracture mechanisms between the two regions are quite different. In the crack propagation region, there are many striationlike bands, which are induced by the gradual propagation of the fatigue crack. However, no veinlike fracture features were observed. In the final fast fracture region, the fracture feature mainly consists of a veinlike structure, which is identical to that observed under tensile fracture.

REFERENCES

1. W.L. Johnson, MRS Bull. **24**(10), 42 (1999).
2. A. Inoue, Acta Mater. **48,** 279 (2000).
3. C.A. Pampillo, Scripta Metall. **6,** 915 (1972).
4. H.J. Leamy, H.S. Chen, and T.T. Wang, Metall. Trans. A **3,** 699 (1972).

5. C.A. Pampillo, J. Mater. Sci. **10,** 1194 (1975).

6. F. Spaepen, Acta Metall. **25,** 407 (1977).

7. A.S. Argon, Acta Metall. **27,** 47 (1979).

8. P.E. Donovan and W.M. Stobbs, Acta Metall. **29,** 1419 (1981).

9. P.E. Donovan, Mater. Sci. Eng. **98,** 487 (1988).

10. P.S. Steif, F. Spaepen, and J.W. Hutchinson, Acta Metall. **30,** 447 (1982).

11. P.E. Donovan, Acta Metall. **37,** 445 (1989).

12. Y. Leng and T.H. Courtney, J. Mater. Sci. **26,** 588 (1991).

13. C. Fan, and A. Inoue, Appl. Phys. Lett. **77,** 46 (2000).

14. A. Inoue, Adv. Eng. Mater. **3,** 669 (2001).

15. J. Eckert, A. Leonhard, B. Weiβ, M. Heilmaier, and L. Schultz, Adv. Eng. Mater. **3,** 41 (2001).

16. R.D. Conner, R.B. Dandliker, and W.L. Johnson, Acta Mater. **46,** 6089 (1998).

17. H. Choi-Yim, R. Busch, U. Koster, and W.L. Johnson, Acta Mater. **47,** 2455 (1999).

18. H. Choi-Yim, J. Schroers, and W.L. Johnson, Appl. Phys. Lett. **80,** 1906 (2002).

19. C.C. Hays, C.P. Kim, and W.L. Johnson, Phys. Rev. Lett. **84,** 2901 (2000).

20. U. Kühn, J. Eckert, N. Mattern, and L. Schultz, Appl. Phys. Lett. **80,** 2478 (2002).

21. R.W.K. Honeycombe, *Plastic Deformation of Metals* (Cambridge Press, 1969).

22. S. Takayama, Scripta Metall. **13,** 463 (1979).

23. P. Lowhaphandu, S.L. Montgomery, and J.J. Lewandowski, Scripta Mater. **41,** 19 (1999).

24. W.J. Wright, R. Saha, and W.D. Nix, Mater. Trans. **42,** 642 (2001).

25. G. He, J. Lu, Z. Bian, D.J. Chen, G.L. Chen, G.H. Tu, and G.J. Chen, Mater. Trans. **42,** 356 (2001).

26. A. Inoue, W. Zhang, T. Zhang, and K. Kurosaka, Acta Mater. **49,** 2645 (2001).

27. C.T. Liu, L. Heatherly, D.S. Easton, C.A. Carmichael, J.H. Schneibel, C.H. Chen, J.L. Wright, M.H. Yoo, J.A. Horton, and A. Inoue, Metall. Mater. Trans. A**29,** 1811 (1998).

28. T. Mukai, T.G. Nieh, Y. Kawamura, A. Inoue, and K. Higashi, Scripta Mater. **46,** 43 (2002).

29. A.T. Alpas, L. Edwards, and C.N. Neid, Mater. Sci. Eng. **98,** 501 (1988).

30. C.J. Gilbert, R.O. Ritchie, and W.L. Johnson, Appl. Phys. Lett. **71,** 476 (1997).

31. Y. Yokoyama, N. Nishiyama, K. Fukaura, and H. Sunada, Mater. Trans., JIM **41,** 675 (2000).

32. K.M. Flores and R.H. Dauskardt, J. Mater. Res. **14,** 638 (1999).

33. C.J. Gilbert, V. Schroeder, and R.O. Ritchie, Metall. Mater. Trans. A**30,** 1739 (1999).

34. A. Tatschl, C.J. Gilbert, V. Schroeder, R. Pippan, and R.O. Ritchie, J. Mater. Res. **15,** 898 (2000).

35. K. Fujita, A. Inoue, and T. Zhang, Scripta Mater. **44,** 1629 (2001).

36. V. Schroeder, C.J. Gilbert, and R.O. Ritchie, Mater. Sci. Eng. A**317,** 145 (2001).

37. J.A. Verduzco, R.J. Hand, and H.A. Davies, Int. J. Fatigue **24,** 1089 (2002).

38. U. Essmann, U. Gosele, and H. Mughrabi, Philos. Mag. **44,** 405 (1981).

39. A. Hunsche and P. Neumann, Acta Metall. **34,** 207 (1986).

40. M. Saletore and R. Taggart, Mater. Sci. Eng. **36,** 259 (1978).

41. Z.F. Zhang, Z.G. Wang, and Z.M. Sun, Acta Mater. **48,** 2875 (2001).

42. H. Mughrabi, F. Ackermann, and K. Herz, ASTM STP, **81,** 5 (1981).

43. Z.F. Zhang and Z.G. Wang, Philos. Mag. Lett. **80,** 483 (2000).

44. A.F. Gourgues, Mater. Sci. Technol **18,** 119 (2002).

45. J. Eckert, U. Kühn, N. Mattern, A. Reger-Leonhard, and M. Heilmaier, Scripta Mater. **44,** 1587 (2001).

46. Y. Kawamura, T. Shibata, A. Inoue, and T. Masumoto, Scripta Mater. **37,** 431 (1997).

47. S. Suresh, *Fatigue of Materials,* 2nd ed. (Cambridge Press, 1998).

48. T. Zhang and A. Inoue, Mater. Trans., JIM **39,** 1230 (1998).

49. M.C. Gao, R.E. Hackenburg, and G.J. Shiflet, Mater. Trans. **42,** 1741 (2002).

50. T.C. Hufnagel, P. El-Deiry, and R.P. Vinci, Scripta Mater. **43,** 1071 (2000).